PREDICTING EARTHQUAKE POTENTIAL THROUGH MORPHODEFORMATION MODELING USING SENTINEL-1A IMAGERY IN THE SINGKARAK SEGMENT, INDONESIA

Triyatno TRIYATNO [1*], Dipo CAESARIO [1], Febriandi FEBRIANDI [1], Beni AULIA [1], Azhari SYARIEF [1]

DOI: 10.21163/GT_2025.202.12

ABSTRACT

This study aims to analyze geological and geomorphological conditions, develop a morphodeformation model, and predict potential magnitude, epicenter depth, and Peak Ground Acceleration (PGA) values in the Singkarak Segment, West Sumatra, Indonesia. The Singkarak Segment, intersected by the active Sumatran Great Fault and influenced by nearby Mount Marapi, exhibits high seismic risk due to its complex tectonic and volcanic settings. The research employed multi-phase spatial analysis using secondary data sources, including Sentinel-1A satellite imagery, Digital Elevation Model Nasional (DEMNAS), geological and geomorphological maps from the Indonesian Geospatial Information Agency, and seismic records from the United States Geological Survey (USGS). Morphodeformation was analyzed using Sentinel Application Platform (SNAP) for radar data processing. ArcGIS, including kriging interpolation and raster calculator, was used to model spatial variations in earthquake magnitude, epicenter depth, and PGA. Results showed denudational and fluvial landforms are most susceptible to seismic activity, with magnitudes ranging from 3.00 to 6.39 Mw and PGA values up to 368.83 gal. The highest magnitude events (≥6.0 Mw) and strongest ground accelerations were concentrated in central and southern zones. Morphodeformation analysis indicated vertical displacements of −0.52 to +0.20 mm (2019–2023) and increased activity in 2023–2024, with values ranging from −0.85 to +0.45 mm. Shallow epicenter depths (18.37–36.64 km) dominated the area, particularly within denudational and fluvial terrains. In conclusion, integrating geological, geomorphological, and deformation modeling confirms that the Singkarak Segment is an active and vulnerable seismic zone. The findings underscore the importance of incorporating morphodeformation and spatial modeling in earthquake risk mitigation, land-use planning, and infrastructure resilience in tectonically dynamic areas.

***Key-words**: Morphodeformation; Earthquake Hazard; PGA; Kriging; Singkarak Segment.*

1. INTRODUCTION

Earthquakes represent one of the most devastating natural disasters, frequently resulting in substantial losses for communities, including both property damage and loss of human life (Razi et al., 2023; Samsonov et al., 2024). These catastrophic events predominantly occur along active fault lines, particularly in areas underlain by geologically weak or fractured rock formations that are less capable of withstanding seismic stress (Appel & Pebesma, 2020; Huang et al., 2022; Jarder et al., 2024). Due to earthquakes' unpredictable and sudden onset, populations are often caught unprepared, amplifying the impact and limiting emergency response effectiveness (Arlym et al., 2019; Hermon et al., 2020; Yang et al., 2022). Earthquakes cause direct destruction and long-term socio-economic disruption by displacing communities, damaging infrastructure, and interrupting essential services such as water supply, electricity, and transportation. One of the areas with significant potential for earthquake-related disasters is the area surrounding Lake Singkarak. Located in West Sumatra Province, Indonesia, Lake Singkarak is classified as a tectonic lake (Novianti et al., 2023), meaning its formation is closely tied to tectonic processes. A major geological structure, the Sumatran Fault, commonly called the Semangko Fault, runs through this area. This extensive fault system stretches from Semangko Bay in Lampung Province to the Alas Valley in Aceh Province, spanning the entire western spine of Sumatra (Guntoro et al., 2024).

---

[1]*Department of Geography, Universitas Negeri Padang, Padang, Indonesia, (TT) triyatno@fis.unp.ac.id, (DC) caesariodipo@fis.unp.ac.id, (FF) andi_geografi@fis.unp.ac.id, (BA) beniaulia@fis.unp.ac.id, (AS) azharief@fis.unp.ac.id. *Corresponding author email: triyatno@fis.unp.ac.id*

The section that passes through Lake Singkarak is known as the Singkarak Segment (Amir et al., 2021). The Singkarak Segment is recognized as one of the most active fault segments on Sumatra. Notably, it lies near Mount Marapi, one of Indonesia's active stratovolcanoes (Rozaki et al., 2024; Hermon et al., 2019). Sumatra has experienced devastating earthquake events, including the 2004 Indian Ocean earthquake and tsunami, which claimed over 230,000 lives, and the 2009 Padang earthquake, which caused widespread damage and over 1,100 fatalities (Chang Seng, 2010; Ranke, 2016). These disasters underscore the urgent need for advanced geospatial modeling and seismic risk assessment, particularly in tectonically active segments like Singkarak. The Semangko Fault produces structural landforms such as fault scarps and lineaments, and volcanic processes from Mount Marapi contribute to volcanic landforms, including cones and pyroclastic deposits. Landform types indicate dynamic geological processes and underscore dual exposure to seismic and volcanic hazards. As such, the area around Lake Singkarak requires continuous geological monitoring and disaster risk management strategies to mitigate potential impacts, including secondary hazards like landslides or lahars. Previous studies have explored natural disasters such as earthquakes (Feng et al., 2024), as well as surface deformation of the earth's crust (Gama et al., 2017; Ghaderpour et al., 2024). However, limited attention has been given to integrated studies of morphodeformation as a method to predict potential earthquake magnitude, epicenter depth, and Peak Ground Acceleration (PGA) values in high-risk areas like the Singkarak Segment, where seismic activity intersects with complex geological and geomorphological characteristics. This study combines several techniques, including kriging interpolation, algebraic map analysis using raster calculator tools in ArcGIS, and satellite-based deformation modeling with Sentinel Application Platform (SNAP) software. This study aims to analyze geological and geomorphological conditions, develop a morphodeformation model, and predict potential magnitude, epicenter depth, and PGA values in the Singkarak Segment area. The novelty of this study lies in its ability to quantify and map the relationship between vertical morphodeformation (uplift and subsidence) and seismic parameters (magnitude, depth, PGA) within a tectono-volcanic zone

2. STUDY AREA

This study was conducted in the Singkarak Segment area, which is geographically located at coordinates 0°36′44.17″S and 100°32′21.14″E, covering the administrative areas of Tanah Datar Regency and Solok Regency, West Sumatra Province, Indonesia, with a surface height of 363.5 m above sea level. For more details, see **Fig 1**.

Fig. 1. Location map in the Singkarak Segment, West Sumatra, Indonesia

The map in **Fig** 1 above shows the of the Singkarak Segment in the regional context of Sumatra Island and shows its strategic position on the Semangko Fault line. The Sumatra region with provincial boundaries and active fault lines extending from Semangko Bay in Lampung to Alas Valley in Aceh. The study area is marked with a red box, showing the focus area in the regional tectonic context. This map serves as an important basis in demonstrating the spatial relationship between the study site and the main tectonic system of Sumatra, while also emphasizing the need for integrated deformation mapping and morphodeformation studies in this earthquake-prone area.

3. DATA AND METHODS

3.1. Data Sources

The data utilized in this study were gathered from multiple sources to facilitate spatial and deformation modeling. **Table 1** presents the datasets employed, which include satellite imagery, digital elevation models, seismic data, and thematic maps concerning geology and geomorphology. Each dataset is provided with its corresponding source and a concise explanation of its relevance to the study.

Table 1.

Study data and sources.

No	Data	Source	Information
1	Sentinel-1A Imagery	United States Geological Survey (USGS)	Deformation modeling
2	Earthquake Data		Spatial modeling of magnitude, epicenter depth, and PGA
3	Digital Elevation Model Nasional (DEMNAS)	Indonesian Geospatial Information Agency	Hillshade modeling
4	Geomorphological Map		Spatial distribution of landforms
5	Geological Map	Indonesian Ministry of Energy and Mineral Resources	Spatial distribution of lithological units

3.2. Study Process

The study on morphological deformation in the Singkarak segment was carried out through several structured phases. The first stage involved acquiring secondary data from authorized institutions, such as Sentinel satellite imagery obtained via the USGS, Digital Elevation Model Nasional (DEMNAS) elevation data, geological and geomorphological maps from the Indonesian Geospatial Information Agency, and earthquake records also retrieved from the USGS. The next phase focused on spatially interpolating earthquake epicenter data using the ordinary kriging method within ArcGIS software, selected for its robustness in estimating spatial autocorrelation in geophysical datasets**.** Simultaneously, Sentinel-1A radar imagery was analyzed using SNAP software to assess deformation levels within the Singkarak segment. Subsequent analytical steps involved algebraic overlay analysis using the Raster Calculator in ArcGIS, integrating interpolated seismic parameters with deformation data to construct a composite morphodeformation model. To develop a comprehensive morphological deformation model for the Singkarak segment, the integrated datasets, including deformation distribution, earthquake magnitudes, epicenter depths, PGA values, and geological-geomorphological layers, were processed using algebraic raster modeling techniques. This geospatial approach, based on kriging interpolation, facilitated the prediction of seismic characteristics such as earthquake magnitudes, epicenter locations, and PGA values across different geomorphological units in the study area. For a detailed illustration, please refer to **Fig 2**.

To assess the geospatial distribution of geological and geomorphological features within the Singkarak segment, geological maps issued by the Geological Agency under the Indonesian Ministry of Energy and Mineral Resources, along with geomorphological maps from the Indonesian Geospatial Information Agency, were employed as primary reference data. The geological features considered in this analysis include lithological units such as volcanic rocks (e.g., andesite, lava, tuff), sedimentary formations (e.g., limestone, alluvium), and intrusive bodies (e.g., granite, diorite).

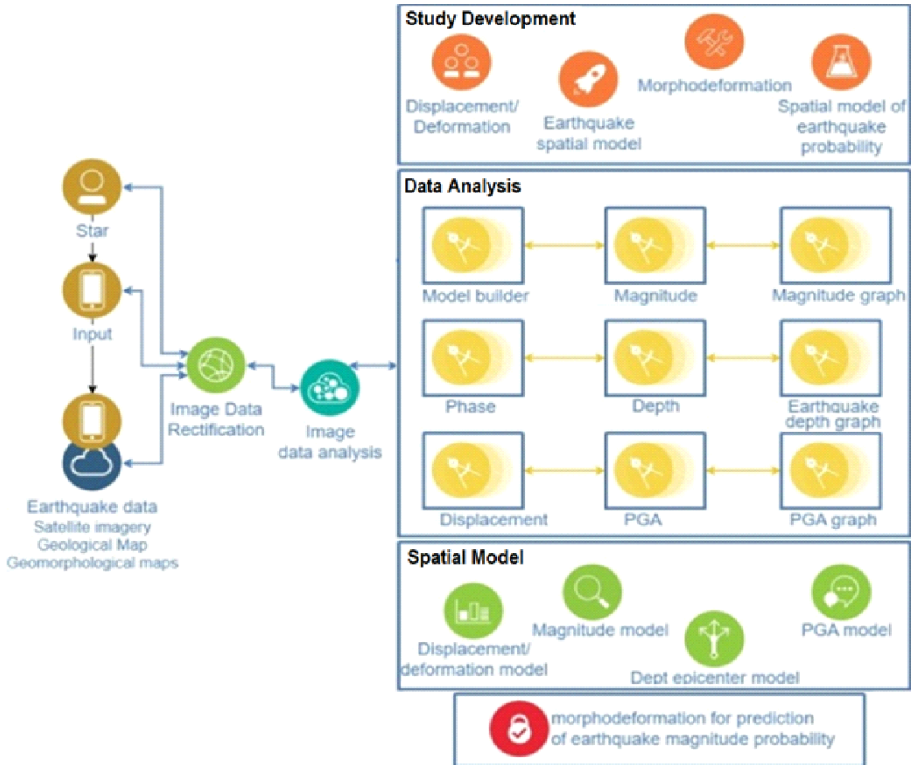

Fig. 2. Morphodeformation-Based Earthquake Spatial Modeling Workflow.

Meanwhile, the geomorphological features encompass denudational, fluvial, karst, volcanic, and structural landforms. The delineation of the study area covers the Singkarak Segment, geographically bounded by coordinates 0°36′44.17″S and 100°32′21.14″E, and administratively includes Tanah Datar and Solok Regencies in West Sumatra Province, Indonesia.

These datasets were integrated into the image analysis workflow (refer to the Image Data Analysis and Study Development sections in **Fig 2**). To generate these spatial models, the kriging interpolation technique was applied to the earthquake dataset, as illustrated in the Data Analysis section of the diagram. This analytical step supported the development of earthquake magnitude models, epicenter depth models, and the PGA model, which collectively contributed to the construction of a comprehensive spatial morphodeformation model. The spatial interpolation process was carried out following the methodology outlined by Njifon & Schuhmacher (2024), Atkinson et al. (2022); Guo et al. (2022), using the following equation:

$$Z = (x_p) = \sum_{i=1}^{n} \quad \lambda_{i\,.}\, Z\,(x_i)\; with \;\; \sum_{i=1}^{n} \quad \lambda_{i\,.} = 1 \qquad (1)$$

where $\lambda_{i\,.}$ represents the kriging weight, and $Z\,(x_i)$ is the observed value at a known location, while $Z(x_p)$ denotes the estimated value at an unknown location x_p.

Inverse Distance Weighting (IDW) is a deterministic interpolation method used to estimate the value of a variable at unsampled points based on the weighted average of nearby known values. To calculate the weight coefficients in kriging interpolation, the procedure follows the approach described by Triyatno et al. (2020); Payares-Garcia et al. (2023); Suesse et al. (2023), using the following equation.

$$\lambda_{i\,.} = \frac{D_i^{-a}}{\sum_{i=1}^{n} D_i^{-a}} \quad (2)$$

where: $\lambda_{i\,.}$ denotes the weight assigned to point i, D_i represents the distance from point i to the location of the unknown value, and the weight is raised to the tenth power to emphasize the influence of proximity in the interpolation process (Cimellaro et al., 2024).

To quantify the extent of ground deformation in the Singkarak segment, the following formulations were applied based on the approaches outlined by Razi et al. (2023).

$$\Delta\varphi_{m.s}^{disp}(T) = \frac{4\pi}{\lambda}\beta_t \Delta v(T) \quad (3)$$

where: $\Delta\varphi(T)$ refers to the target velocity at time T, $\Delta\varphi_{m.s}^{disp}(T)$ denotes the atmospheric phase component, which can be estimated through residual modeling techniques, and $\Delta\varphi_{m.s}^{disp}(T)$ represents the phase noise contribution, derived from Synthetic Aperture Radar (SAR) data conversion and and subsequently excluded from the residual phase model (Babaee et al., 2024).

4. RESULTS

4.1. Morphodeformation using Geomorphological, Geological, and Seismicity Data

To understand the morphotectonic dynamics of the Singkarak segment, this study utilized geomorphological maps, geological maps, and the spatial distribution of earthquake epicenters. These spatial data were analyzed as part of the morphological deformation assessment to determine how landform types and lithological structures influence seismic activity in the area. **Fig 3** shows the geomorphological and geological characteristics of the Singkarak segment, along with the distribution of recorded earthquake points.

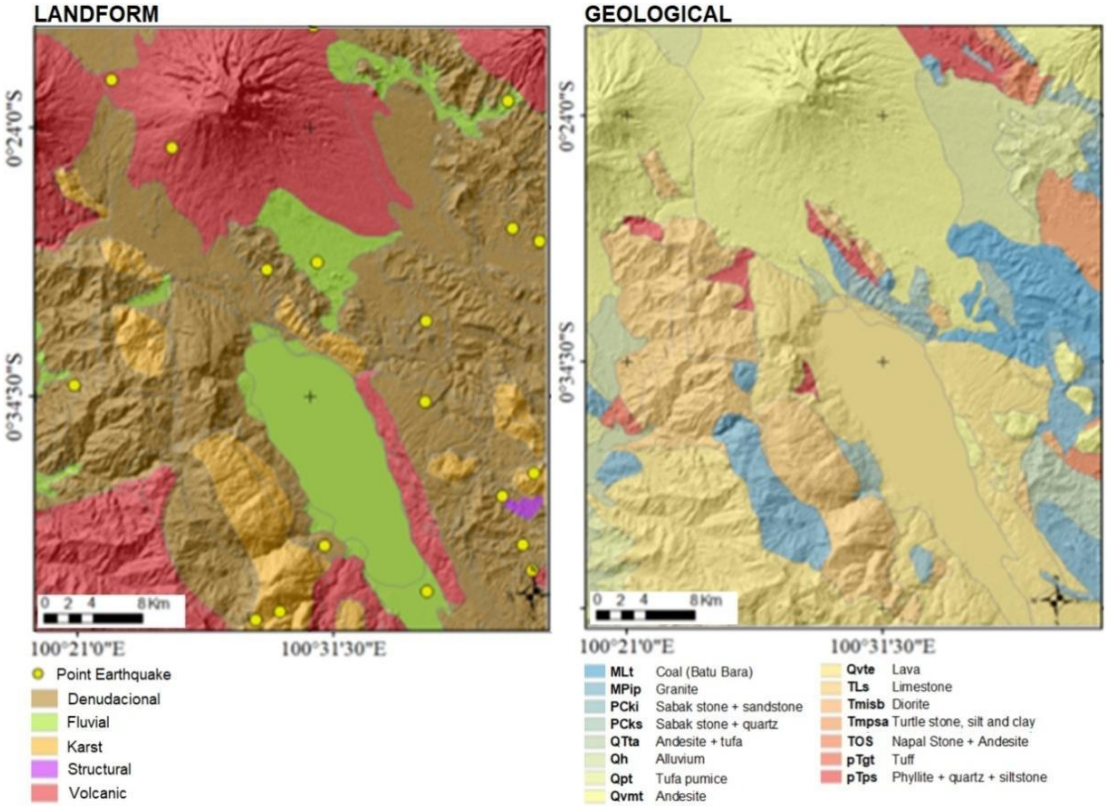

Fig. 3. Geomorphological (left) and Geological (left) Maps of the Singkarak Segment, showing earthquake distribution, surface lithology, and landform units.

The geomorphological map (left) shows that the Singkarak segment comprises various landform units, including denudational, fluvial, karst, volcanic, and structural landforms. Denudational landforms dominate the western and northern areas, while fluvial landforms are concentrated along the low-lying central basin surrounding Lake Singkarak. Volcanic landforms are prominent in the northwestern and southeastern zones. The distribution of earthquake points (shown as yellow dots) appears clustered along the boundary zones between different landforms, particularly where fluvial areas meet denudational and volcanic zones, indicating active deformation fronts. Meanwhile, the geological map (left) reveals a complex assemblage of rock types in the study area. The dominant lithological units include volcanic rocks such as andesite (Qvmt, QTta), lava (Qvte), and tuff (pTgt), as well as sedimentary deposits like limestone (TLs), alluvium (Qh), and phyllite (pTps). Intrusive rocks such as granite (MPip) and diorite (Tmisb) are also identified. Zones composed of andesite and tuff are more susceptible to ground uplift and correlate with areas showing higher earthquake frequencies, while sediment-dominated units such as alluvium tend to associate with subsidence. The spatial distribution and magnitude model were developed using ArcGIS to create predictive spatial representations of earthquake behavior within the study area. The interpolation results in **Fig 4** show an overview of both the magnitude intensity and the distribution of epicenters across the Singkarak Segment.

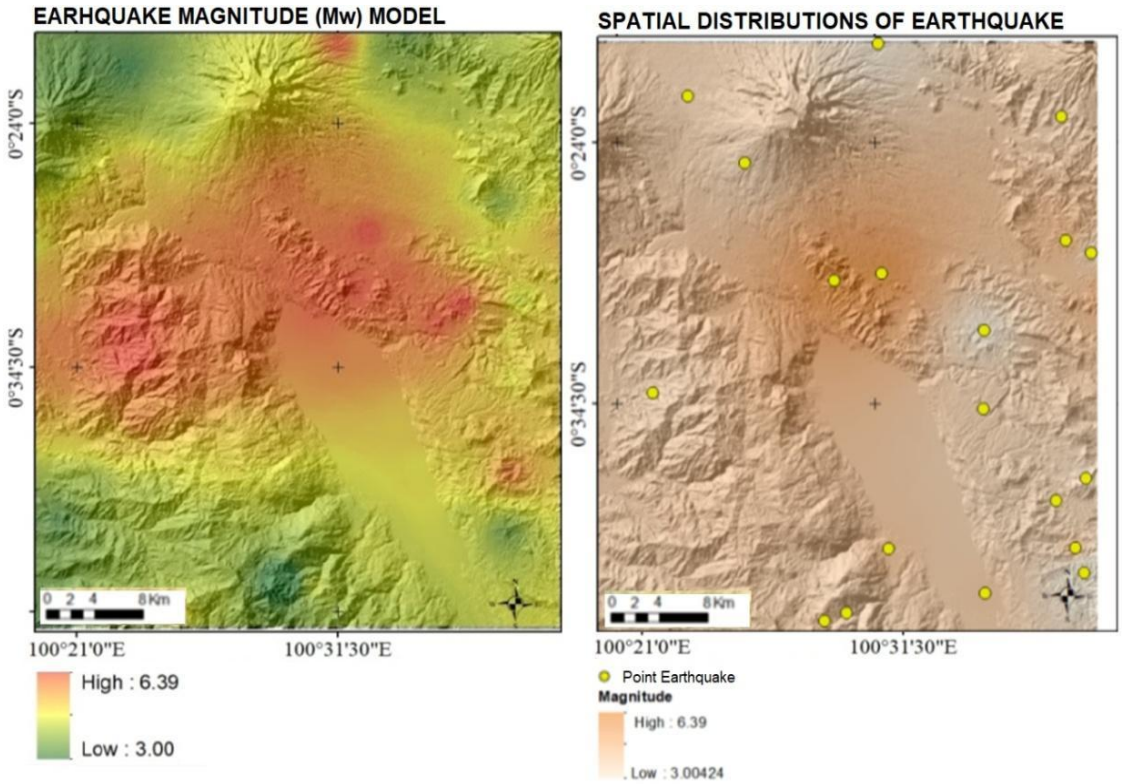

Fig. 4. Earthquake Magnitude Model (left) and Spatial Distribution of Earthquake Epicenters (right) in the Singkarak Segment.

Fig 4 above displays two key outputs of the spatial earthquake analysis. The left map shows the Earthquake Magnitude (Mw) Model, while the right map depicts the Spatial Distribution of Earthquake Epicenters. Based on the magnitude model, the intensity of earthquakes ranges from 3.00 Mw to 6.39 Mw, with higher magnitudes (≥ 6.0 Mw) predominantly concentrated in the central part of the study area. These zones correspond with areas characterized by complex geological and geomorphological transitions, particularly where denudational and volcanic landforms intersect. The

right map further supports these findings, showing that the epicenters of earthquakes are scattered across the segment but tend to cluster in the central and southeastern areas. The presence of multiple epicenters in this area indicates zones of high tectonic stress, likely associated with active fault segments such as the Semangko Fault that bisects the study area. Meanwhile, lower-magnitude events (3.0–4.5 Mw) are more widely dispersed, particularly in the northern and southern zones, which are dominated by softer lithologies such as alluvium and tufa pumice. To further support the morphological deformation analysis in the Singkarak Segment, this study includes a geological and morphological cross-section along the A–B transect line. This cross-section was developed by integrating surface geological data with subsurface interpretations derived from tectonic structures, fault orientations, and lithological layers. The tectonic block on the eastern side of the fault appears uplifted and intruded by larger magmatic bodies, while the western block, though elevated, is more eroded and composed of more sedimentary deposits. **Fig 5** shows the contour map, 3D terrain model, and longitudinal profile of the study area, providing a detailed geomorphological characterization that complements the geological and seismic analysis.

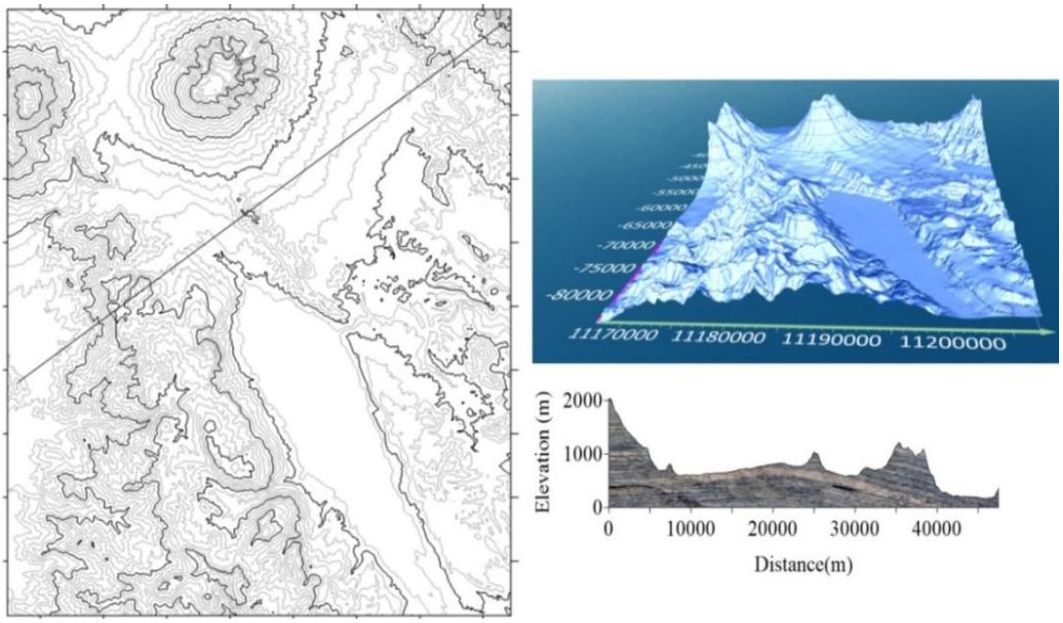

Fig. 5. Contour Line Map (left), 3D Terrain Model (top right), and Longitudinal Elevation Profile (bottom right) of the Singkarak Segment, illustrating morphological variation and elevation gradients across

Fig 5 above shows the morphological structure of the Singkarak Segment through three complementary visualizations: a contour map (left), a 3D surface model (top right), and a longitudinal topographic cross-section (bottom right). The contour lines show dense clustering in some zones, indicating steep terrain, while wider spacing reveals gentler slopes. The 3D model highlights elevation contrasts across the segment, emphasizing mountainous areas, valleys, and basins surrounding Lake Singkarak. The elevation profile shows that the area consists of asymmetrical blocks ranging from near 0 m to above 2,000 m, forming a pronounced morphological tilt from east to west and vice versa. This aligns with the geological structure governed by the Semangko Fault, which segments the area into uplifted and subsided blocks. The slope angle, ranging from 23° to 45°, reflects the tectonically active nature of the region, where faulting and magmatic processes shape the surface. Overall, this cross-section confirms the complex tectono-morphological dynamics of the Singkarak segment, reinforcing deformation and seismic model outputs from kriging and Sentinel-1A radar analysis. **Tables 2** and **3**, and **Fig 6** show the formation distribution for 2019–2023 and 2023–2024. This analysis identifies uplift or subsidence zones critical to understanding regional tectonic behavior.

Table 2.

Morphodeformation Frequency Distribution in 2019–2023.

Interval Morphodeformation (cm)	Denudasional	Fluvial	Karst	Volcanic
−0.398 – −0.264	4	1	4	2
−0.265 – −0.131	12	3	2	2
−0.132 – 0.002	13	6	3	15
0.003 – 0.137	15	3	2	13

Source: Data Analytics 2024.

Table 3.

Morphodeformation Frequency Distribution in 2023–2024.

Interval Morphodeformation (cm)	Denudasional	Fluvial	Karst	Volcanic
−0.748 – −0.503	1	2	0	3
−0.504 – −0.259	22	4	1	8
−0.260 – −0.015	13	5	4	12
−0.016 – 0.229	8	4	6	9

Source: Data Analytics 2024.

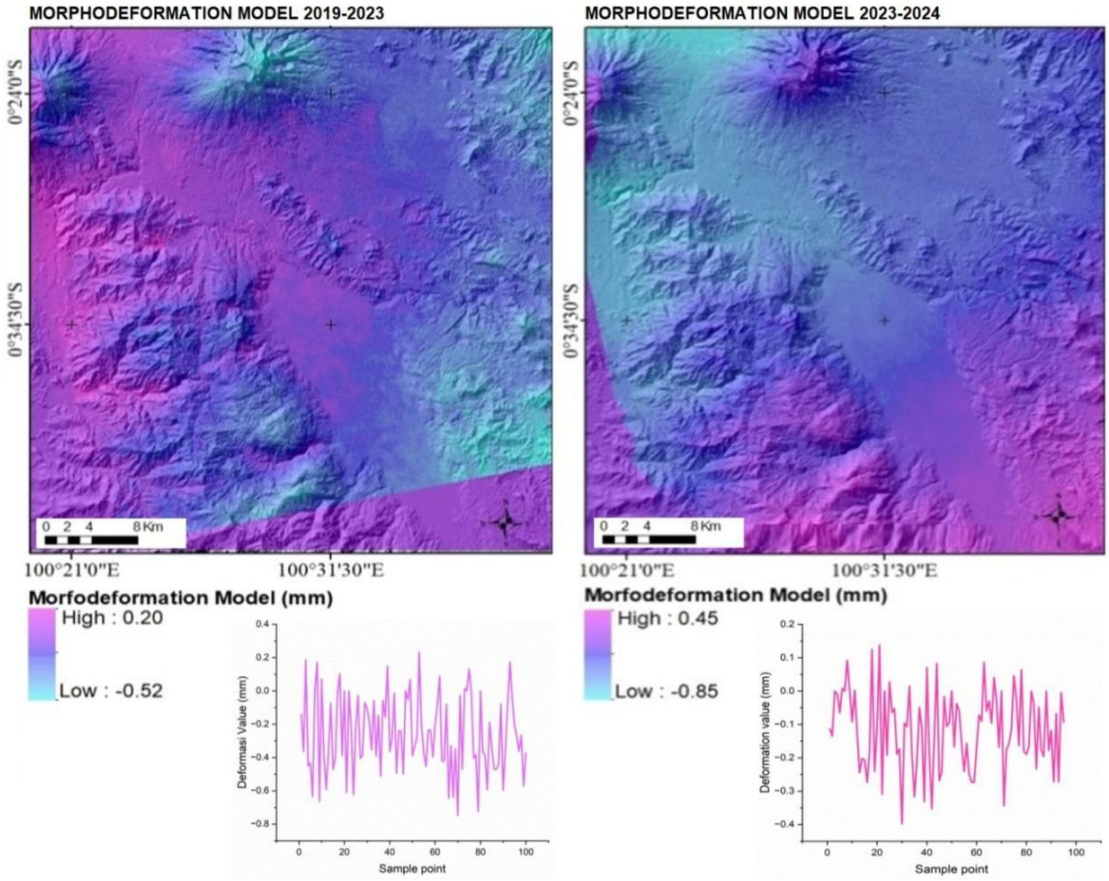

Fig. 6. Comparison of Morphodeformation Models in the Singkarak Segment for 2019–2023 (left) and 2023–2024 (right), showing uplift and subsidence patterns in mm based on Sentinel-1A analysis.

Fig 6 above shows the Morphodeformation Model for two timeframes. During the 2019–2023 period, deformation values ranged from 0.52 mm (subsidence) to +0.20 mm (uplift). In contrast, during the 2023–2024 period, the deformation intensified, with subsidence reaching −0.85 mm and uplift rising to +0.45 mm. The corresponding statistical frequencies for each deformation interval and

geomorphological unit are shown in **Tables 2 and 3**. It is observed that during 2019–2023, deformation was relatively balanced, with uplift more prominent in volcanic and denudational landforms. In 2023–2024, deformation frequency rose sharply, especially in denudational units, which showed greater subsidence (−0.504 to −0.259 cm). This trend indicates an intensifying tectonic regime in the Singkarak Segment, particularly in boundary zones where uplift and subsidence overlap.

4.2. Spatial Modeling of Earthquake Magnitude, Epicenter Depth, and PGA

This study utilized kriging interpolation and spatial randomization techniques applied to earthquake magnitude, epicenter depth, and PGA data to estimate the spatial potential of earthquake occurrence in the Singkarak Segment. The spatial model produced allows for the simulation of high-risk zones across the segment, reflecting areas with similar seismic characteristics based on observed geophysical parameters. **Fig 7** shows the spatial distribution of Mw, helping to identify areas with higher earthquake susceptibility.

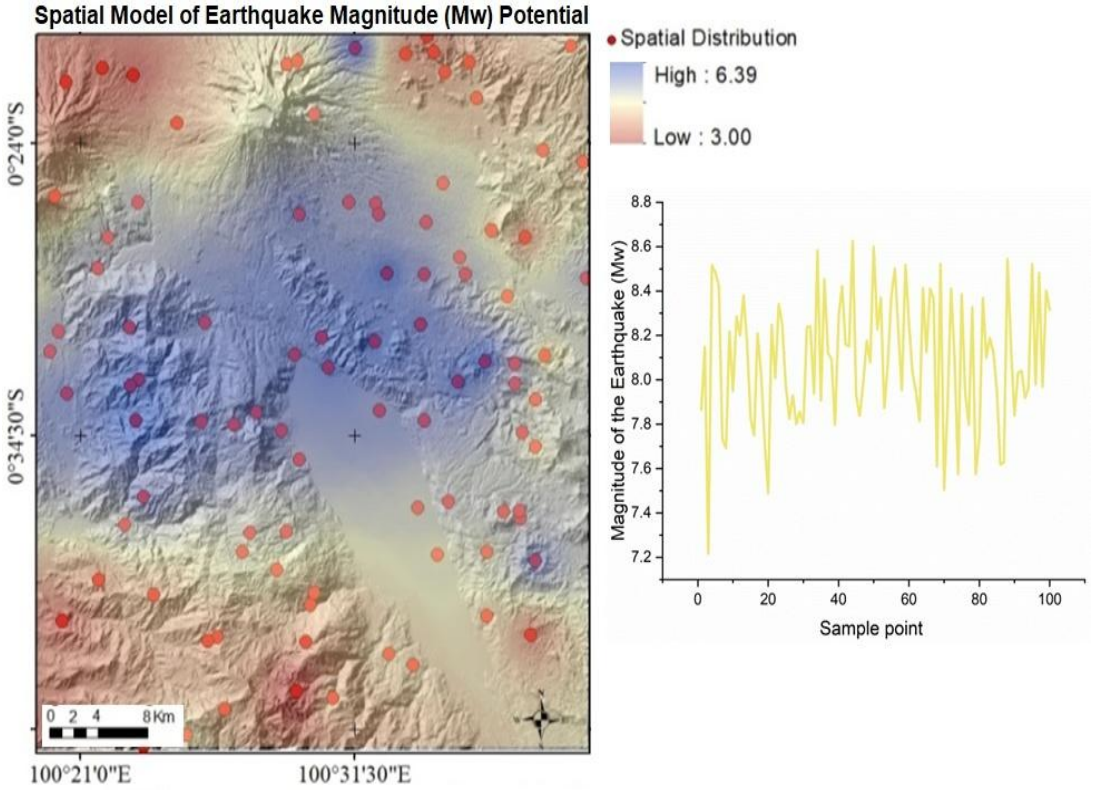

Fig. 7. Spatial distribution of estimated Mw in the Singkarak Segment using kriging interpolation (left) and magnitude variation across sample points (right).

Fig 7 shows a spatial model of Mw across the Singkarak Segment. The color gradient represents estimated magnitudes from 3.00 Mw (blue) to 6.39 Mw (red), while red and blue dots indicate distribution points used in interpolation. Higher-magnitude zones (≥6.0 Mw) are concentrated in the central and southern parts, aligning with fluvial and denudational landforms where structural deformation is more active. In contrast, lower-magnitude zones (≈3.0 Mw) appear in the northern, eastern, and far southern areas, dominated by volcanic, denudational, or karstic landforms. The line graph shows magnitude variation across sample points, indicating fluctuating yet generally high values and non-uniform seismic potential. Geomorphological transitions, such as between fluvial and volcanic terrain, often act as seismic accumulation or release zones. For more details, see **Table 4** below.

Table 4.

Frequency Distribution of Earthquake Magnitudes (Mw).

Magnitude Interval (Mw)	Denudasional	Fluvial	Karst	Volcanic
7.216 – 7.568	1	0	2	1
7.569 – 7.921	5	2	3	12
7.921 – 8.273	19	5	6	14
8.274 – 8.625	19	6	0	5

Source: Data Analytics 2024.

Table 4 shows that the highest frequency of large-Mw (7.921–8.625 Mw) earthquakes occurred in denudational landforms, with 19 events recorded in each upper interval. Volcanic landforms also showed notable seismicity, especially in the 7.569–8.273 Mw range, with 12 and 14 events. Karst and fluvial units experienced fewer but still significant events, indicating that all geomorphological settings in the Singkarak Segment are affected by earthquake activity at different intensities. Epicenter depth is critical for surface damage, ranging from 18.37 to 91.41 km, indicating shallow to intermediate-depth events. **Fig 8** shows the spatial distribution and depth variation of epicenters derived from seismic modeling and interpolation.

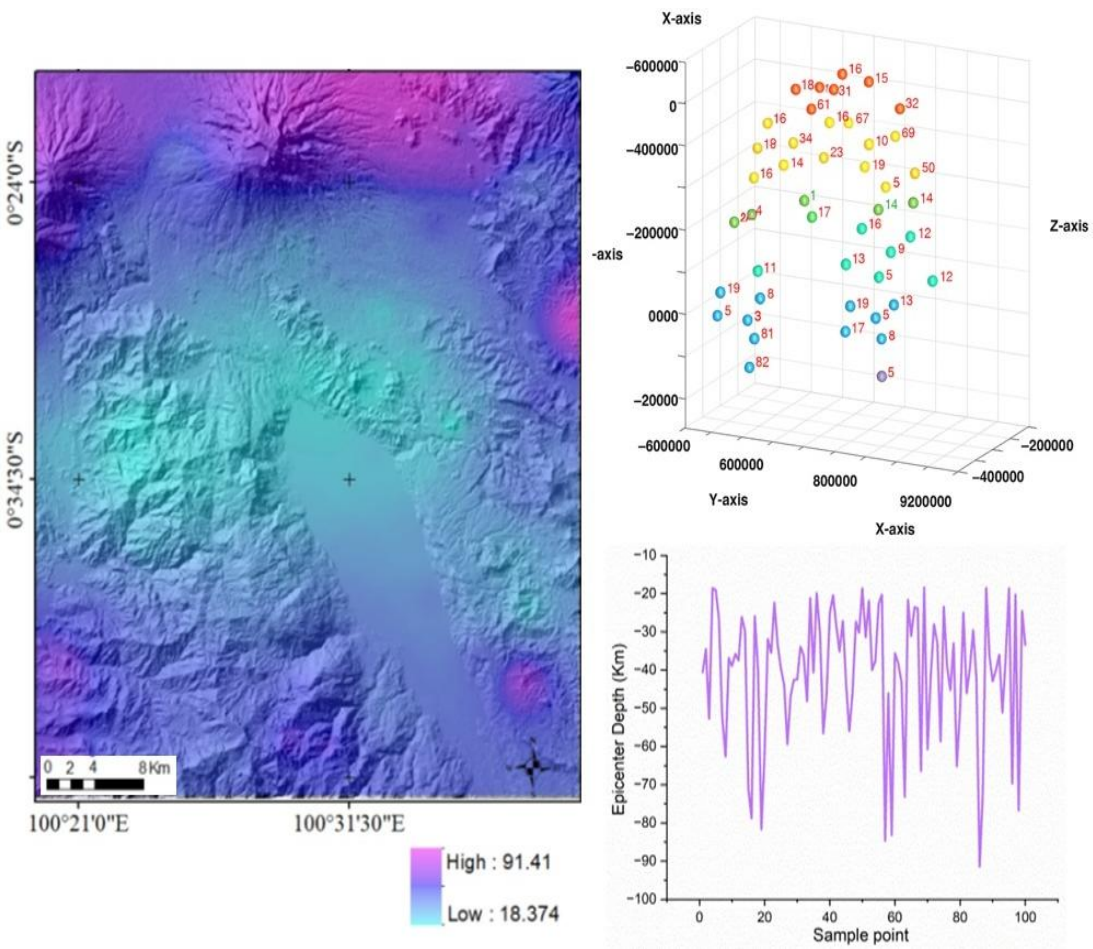

Fig. 8. Spatial model of earthquake epicenter depth in the Singkarak Segment (left), 3D scatter plot of epicenter distribution (top right), and depth variation across sample points (bottom right).

The map (left) shows the spatial model of epicenter depth, where shallower earthquakes (18.37–36.64 km) dominate the central part of the Singkarak Segment, marked by cyan to blue zones. In contrast, deeper events are concentrated toward the northern and southeastern flanks, indicated by pink to purple shades. The 3D scatter plot (top right) displays the vertical and horizontal distribution of earthquake epicenters across the segment, confirming seismic stratification at different depths. The line graph (bottom right) illustrates variations in epicenter depth across 100 sample points, showing that most events fall within −20 to −40 km, supporting the conclusion that shallow earthquakes are most prevalent. For more details, see **Table 5** below.

Table 5.

Frequency Distribution of Earthquake Epicenter Depths.

Dept Interval (km)	Denudasional	Fluvial	Karst	Volcanic
-18.36 – -36.64	28	9	6	7
-36.64 – -54.91	5	0	5	13
-54.91 – -73.19	2	3	0	9
-73.19 – -91.47	9	1	0	3

Source: Data Analytics 2024.

Table 5 shows that denudational and fluvial geomorphological units most commonly host shallow epicenters, with 28 and 9 occurrences, respectively, in the depth range of −18.36 to −36.64 km. Volcanic terrains show greater activity at intermediate depths (−36.64 to −73.19 km), indicating tectono-magmatic influences. Most seismic activity in the Singkarak Segment originates at shallow depths, especially in zones affected by faulting and uplift, making them critical for hazard mitigation and spatial planning. Seismic shaking intensity is strongly influenced by geological structure and surface morphology. **Fig 9** shows the PGA spatial model, with a 3D view and graph of PGA variation across sampling points.

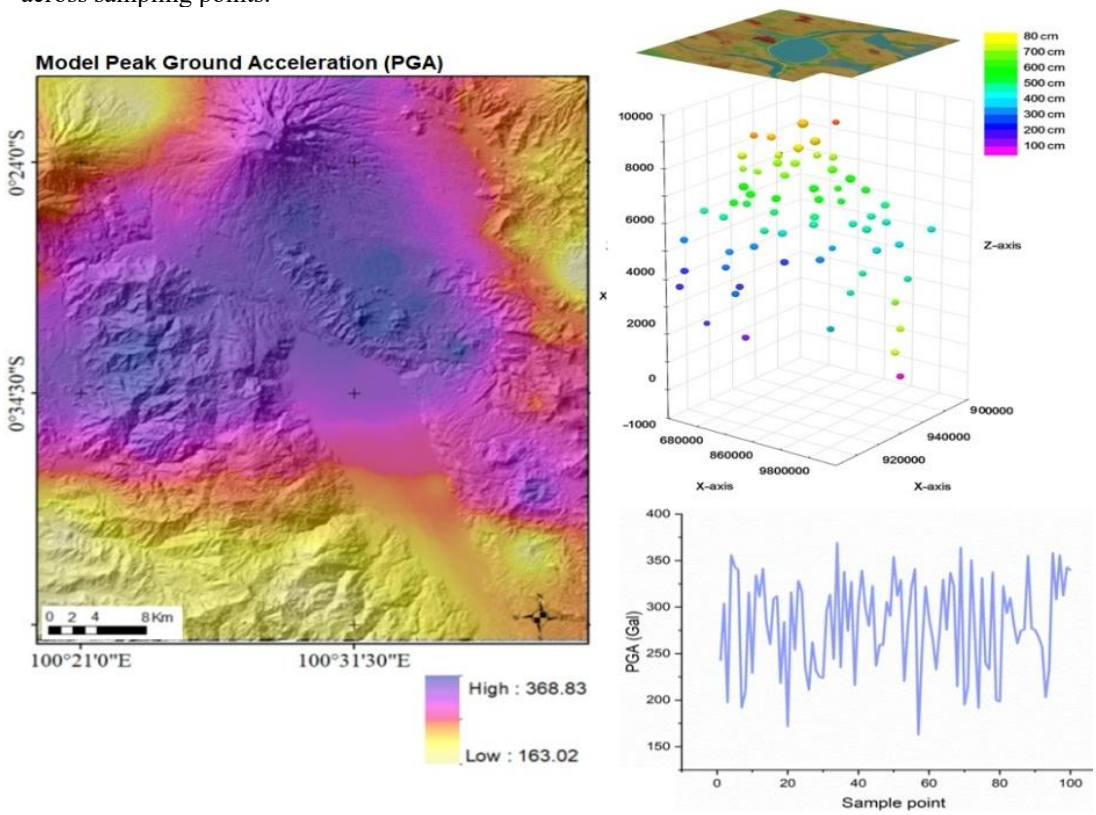

Fig. 9. Spatial model of PGA in the Singkarak Segment (left), 3D distribution of PGA intensity (top right), and PGA variation across sample points (bottom right).

The PGA map (left) shows the spatial distribution of maximum ground acceleration in the Singkarak Segment. The PGA values range from 163.02 gal (low) to 368.83 gal (high). The highest acceleration values are concentrated in the central zone, corresponding to tectonically active areas with fluvial and denudational geomorphological units. These zones also overlap with areas previously identified as having shallow epicenters and significant uplift/subsidence, making them highly vulnerable to strong ground motion. Higher PGA values (yellow to red) are more densely clustered in elevated or fault-affected areas, consistent with the surface model. The line graph (bottom right) confirms PGA fluctuation across 100 sample points, with many points recording values between 250–370 gal, indicating widespread moderate to high seismic acceleration across the segment. Areas with high PGA values are priority zones for earthquake risk reduction strategies, including building reinforcement, land-use planning, and community preparedness. To support the spatial model results of PGA distribution, the following **Table 6** shows a more detailed breakdown of PGA frequency distribution across different geomorphological units in the Singkarak Segment.

Table 6.

Frequency Distribution of PGA.

PGA Interval	Denudasional	Fluvial	Karst	Volcanic
162.98 – 214.47	2	0	1	5
215.00 – 266.49	2	2	3	14
267.00 – 318.49	10	6	4	8
319.00 – 370.49	30	5	3	5

Source: Data Analytics 2024.

Table 6 shows that the highest concentration of PGA values (319.00–370.49 gal) occurs predominantly in denudational landforms, with 30 recorded events, highlighting this unit as the most affected by strong ground motion. These areas are typically characterized by steep slopes and active tectonic deformation, making them highly responsive to seismic wave amplification. Volcanic landforms also exhibit elevated PGA values across all intervals, particularly in the 215.00–266.49 gal range, where 14 occurrences were recorded. This suggests a strong influence of past magmatic activity and fractured rock structures in facilitating seismic energy transmission. Fluvial units, commonly found in low-lying valleys and sedimentary basins, show a moderate distribution of PGA, with 5 occurrences in the highest range, possibly due to sediment amplification effects that intensify ground shaking. Although karst landforms recorded fewer high-PGA events, they still appear in moderate ranges, indicating localized vulnerability depending on structural fractures and subsurface voids. The final overlay results show the distribution of morphodeformation zones, which represent areas where vertical ground deformation (uplift and subsidence) intersects with high seismic vulnerability. These integrated zones combine deformation modeling with seismic hazard indicators, providing essential spatial insight for regional disaster mitigation strategies, land-use planning, and infrastructure resilience development.

4.3. Discussions

Geologically, the area is dominated by sedimentary and volcanic rocks, which are structurally unstable and tectonically complex, increasing the risk of high-magnitude seismic events (Parmar, 2019; Yang et al., 2022). This risk is further exacerbated by the presence of the active Sumatran Great Fault, known locally as the Semangko Fault, and volcanic activity from Mount Marapi, which demonstrated clear tectono-volcanic interaction during its eruption on December 3, 2023 (Istijono et al., 2025). Geomorphologically, the Singkarak Segment consists of fluvial, denudational, and volcanic landforms, each exhibiting different levels of vulnerability (Parmar, 2019; Verma et al., 2020; Zocchi et al., 2025). Earthquake epicenters are concentrated in denudational and volcanic landforms, which also show higher values of earthquake magnitude and PGA (Barbi et al., 2023; Fend & Redenbach, 2024). From 2019 to 2023, deformation ranged between +0.20 mm (uplift) and −0.52 mm (subsidence). During 2023–2024, deformation intensified with uplift reaching +0.45 mm and subsidence deepening to −0.85 mm, particularly along morphological boundaries. The earthquake magnitude ranges from 3.00 to 6.39 Mw, with higher magnitudes (≥6.0 Mw) clustering in the central

and southern parts of the segment, especially in denudational and fluvial areas (Chen & Sharma, 2024; Guo et al., 2022; Heuvelink & Webster, 2022). These magnitudes, though moderate, are capable of causing moderate structural damage, especially in densely populated or poorly built areas (Gama et al., 2017). Most events occur in the shallow range of −18.36 to −36.64 km, concentrated in denudational and fluvial landforms, which intensifies surface shaking. The highest PGA values (up to 368.83 gal) are also found in these units, particularly in the central zone, confirming it as a seismically critical area (Feng et al., 2024). The vulnerability map indicates that high-vulnerability zones are predominantly located in densely populated lowland areas, particularly those with proximity to fault lines and insufficient infrastructure resilience. These regions often feature soft sedimentary soils, limited evacuation routes, and high building density, all of which exacerbate the potential impact of seismic events. Population concentration amplifies exposure and hampers rapid emergency response, making these zones critically susceptible to ground shaking and secondary hazards such as liquefaction or landslides. In conclusion, the integration of geological, geomorphological, and morphodeformation data reveals that the Singkarak Segment is an active deformation zone with considerable earthquake risk. The combination of shallow epicenters, intense PGA, and active tectonics demands priority in hazard mitigation, urban planning, and earthquake preparedness strategies.

5. CONCLUSIONS

This study assessed the geospatial distribution of geological and geomorphological features within the Singkarak Segment, using integrated remote sensing, GIS-based interpolation, and deformation modeling. The key findings indicate that the Singkarak Segment is a morphotectonically active zone characterized by complex lithological compositions and diverse landform units, including denudational, fluvial, volcanic, and karstic terrains. Earthquake epicenters, magnitudes, and PGA values were found to cluster within denudational and fluvial units, where active faulting and deformation are concentrated. Moreover, vertical surface displacement ranging from uplift to subsidence intensified from 2019–2023 to 2023–2024, signaling increasing tectonic stress within the region. The practical implications of these findings are significant for disaster risk reduction and spatial planning in West Sumatra. Identifying zones with high PGA and shallow epicenters enables authorities to prioritize infrastructure retrofitting and land-use regulation in high-risk areas. The morphodeformation modeling approach also provides an early-warning framework that can be updated regularly using new satellite imagery and seismic data. This supports proactive decision-making in earthquake-prone zones like the Singkarak Segment. However, several limitations were encountered in this study. The accuracy of deformation estimates depends on the temporal resolution and atmospheric correction of Sentinel-1A data. Additionally, the kriging interpolation technique, while effective, is influenced by the spatial distribution and density of available seismic records, which may not capture all microseismic activity. Geological and geomorphological maps, though official, may require more frequent updates to reflect landscape changes. Future research should explore machine learning models to complement geostatistical approaches, incorporate near-real-time InSAR datasets, and assess post-seismic ground responses. Furthermore, expanding the study area to include adjacent fault segments may yield broader insights into regional tectonic interactions. Overall, this study contributes a replicable method for integrated seismic hazard mapping in tectonically complex regions.

ACKNOWLEDGEMENTS

The authors would like to express their deepest gratitude to the Universitas Negeri Padang (UNP) for providing study support and access to relevant data and analytical tools. We thank the local governments of Tanah Datar and Solok Regencies for facilitating field visits and providing logistical support during data validation in the Singkarak Segment. This study would not have been possible without the combined efforts and collaboration of institutions and individuals committed to improving earthquake risk reduction and geospatial hazard analysis in Indonesia.

REFERENCES

Amir, H., Bijaksana, S., Dahrin, D., Nugraha, A. D., Arisabaya, I., Pratama, A., & Suryanata, P. B. (2021). Subsurface structure of Sumani segment in the Great Sumatran Fault inferred from magnetic and gravity modeling. Tectonophysics, 821, 229149. https://doi.org/10.1016/j.tecto.2021.229149

Arlym, L., Hermon, D., Lanin, D., Oktorie, O., & Putra, A. (2019). A policy model of preparedness the general hospital in reducing victims of earthquake and tsunami disasters in Siberut Mentawai Island, Indonesia. *International Journal of Recent Technology and Engineering*, 8(3), 89–93. https://doi.org/10.35940/ijrte.C3890.098319

Appel, M., & Pebesma, E. (2020). Spatiotemporal multi-resolution approximations for analyzing global environmental data. Spatial Statistics, 38, 100465. https://doi.org/10.1016/j.spasta.2020.100465

Atkinson, P. M., Stein, A., & Jeganathan, C. (2022). Spatial sampling, data models, spatial scale and ontologies: Interpreting spatial statistics and machine learning applied to satellite optical remote sensing. Spatial Statistics, 50, 100646. https://doi.org/10.1016/j.spasta.2022.100646

Babaee, S., Khalili, M. A., Chirico, R., Sorrentino, A., & Di Martire, D. (2024). Spatiotemporal characterization of the subsidence and change detection in Tehran plain (Iran) using InSAR observations and Landsat 8 satellite imagery. Remote Sensing Applications: Society and Environment, 36, 101290. https://doi.org/10.1016/j.rsase.2024.101290

Barbi, C., Menafoglio, A., & Secchi, P. (2023). An object-oriented approach to the analysis of spatial complex data over stream-network domains. Spatial Statistics, 58, 100784. https://doi.org/10.1016/j.spasta.2023.100784

Chang Seng, D. (2010). Disaster risk preparedness: The role of risk governance, multi-institutional arrangements and polycentric frameworks for a resilient tsunami early warning system in Indonesia (Doctoral dissertation, Rheinische Friedrich-Wilhelms-Universität Bonn).

Chen, Z., & Sharma, P. (2024). Nonparametric statistical analysis of system resilience migration and application for electric distribution structures. Resilient Cities and Structures, 3(3), 92–105. https://doi.org/10.1016/j.rcns.2024.07.005

Cimellaro, G. P., Cardoni, A., & Reinhorn, A. (2024). Modelling infrastructure interdependencies and cascading effects using temporal networks. Resilient Cities and Structures, 3(3), 28–42. https://doi.org/10.1016/j.rcns.2024.05.002

Fend, C., & Redenbach, C. (2024). Nonparametric isotropy test for spatial point processes using random rotations. Spatial Statistics, 64, 100858. https://doi.org/10.1016/j.spasta.2024.100858

Feng, K., Wang, C., & Li, Q. (2024). Evaluating the role of transportation system in community seismic resilience. Resilient Cities and Structures, 3(3), 65–78. https://doi.org/10.1016/j.rcns.2024.05.003

Gama, F. F., Cantone, A., Mura, J. C., Pasquali, P., Paradella, W. R., Dos Santos, A. R., & Silva, G. G. (2017). Monitoring subsidence of open pit iron mines at Carajás Province based on SBAS interferometric technique using TerraSAR-X data. Remote Sensing Applications: Society and Environment, 8, 199–211. https://doi.org/10.1016/j.rsase.2017.09.001

Ghaderpour, E., Mazzanti, P., Bozzano, F., & Scarascia Mugnozza, G. (2024). Ground deformation monitoring via PS-InSAR time series: An industrial zone in Sacco River Valley, central Italy. Remote Sensing Applications: Society and Environment, 34, 101191. https://doi.org/10.1016/j.rsase.2024.101191

Guntoro, A., Triany, N., Adhitama, R., Anugrahadi, A., & Parlindungan, B. (2024). Analysis of tectonic structure and its implications on petroleum systems in the Southeastern arc, Bengkulu Basin, Indonesia. AIP Conference Proceedings, 3019(1), 050004. https://doi.org/10.1063/5.0225803

Guo, X., Kurtek, S., & Bharath, K. (2022). Variograms for kriging and clustering of spatial functional data with phase variation. Spatial Statistics, 51, 100687. https://doi.org/10.1016/j.spasta.2022.100687

Hermon, D., Erianjoni, Dewata, I., Putra, A., & Oktorie, O. (2019). Liquefaction vulnerability analysis as a coastal spatial planning concept in Pariaman City – Indonesia. *International Journal of Recent Technology and Engineering*, 8(2), 4181–4186. https://doi.org/10.35940/ijrte.B3265.078219

Hermon, D., Ganefri., Putra, A., & Oktorie, O. (2019). Characteristics of melanic epipedon based on biosequence in the physiography of Marapi - Singgalang, West Sumatra. *IOP Conference Series: Earth and Environmental Science*, 314(1), 012010. https://doi.org/10.1088/1755-1315/314/1/012010

Hermon, D., Ikhwan., Putra, A., & Oktorie, O. (2020). Spatial analysis of tsunami vulnerability zones as a basic concept of coastal disaster mitigation in development planning of Pariaman City. *Journal of Advanced Research in Dynamical and Control Systems*, 12(7), 681–690. https://doi.org/10.5373/JARDCS/V12SP7/20202158

Heuvelink, G. B. M., & Webster, R. (2022). Spatial statistics and soil mapping: A blossoming partnership under pressure. Spatial Statistics, 50, 100639. https://doi.org/10.1016/j.spasta.2022.100639

Huang, Z., Pitilakis, K., Zhang, D., Tsinidis, G., & Argyroudis, S. (2022). On the effects of salient parameters for an efficient probabilistic seismic loss assessment of tunnels in alluvial soils. Resilient Cities and Structures, 1(3), 24–39. https://doi.org/10.1016/j.rcns.2022.10.006

Istijono, B., Fauzi, M. A. G., Hadiyansyah, D., Andriani, N. S. S., Prastiyo, A., & de Luna Era, M. (2025). Lessons learnt from community preparedness for Mount Merapi and Mount Marapi eruption disasters. E3S Web of Conferences, 604, 13004. https://doi.org/10.1051/e3sconf/202560413004

Jarder, S. L. N., Maruyama, O., & Garciano, L. E. O. (2024). A probabilistic estimation model for seismic physical portfolio loss of a water supply pipeline system. Resilient Cities and Structures, 3(1), 44–54. https://doi.org/10.1016/j.rcns.2024.01.001

Njifon, M.A, & Schuhmacher, D. (2024). Graph convolutional networks for spatial interpolation of correlated data. Spatial Statistics, 60, 100822. https://doi.org/10.1016/j.spasta.2024.100822

Novianti, R., Yuniarti, I., Ajie, G. S., Setiawan, F., Yuerlita, Y., Handoko, U., Triharyuni, S., & Afandi, A. Y. (2023). Towards sustainable management of Lake Singkarak, Indonesia: System analysis and research priorities. IOP Conference Series: Earth and Environmental Science, 1266(1), 012022. https://doi.org/10.1088/1755-1315/1266/1/012022

Parmar, S. (2019). Morphometry analysis using SAGA GIS: A case study of Watershed – 63 of Narmada River, Gujarat, India. International Journal of Engineering Research and Application, 9(2, Series II), 39–51. https://doi.org/10.9790/9622-090203951

Payares-Garcia, D., Osei, F., Mateu, J., & Stein, A. (2023). A Poisson cokriging method for bivariate count data. Spatial Statistics, 57, 100769. https://doi.org/10.1016/j.spasta.2023.100769

Ranke, U. (2016). Natural disaster risk management: Geosciences and social responsibility. Springer.

Razi, P., Sumantyo, J. T. S., Chua, M. Y., Ganefri, Perissin, D., & Tadono, T. (2023). Monitoring of tectonic deformation in the seismic gap of the Mentawai Islands using ALOS-1 and ALOS-2. Remote Sensing Applications: Society and Environment, 30, 100973. https://doi.org/10.1016/j.rsase.2023.100973

Rozaki, Z., Aini, N. N., Kamarudin, M. F., & Triyono, T. (2024). Developing farmers' community resilience in the volcanic area of Mount Merapi, Indonesia. Diyala Agricultural Sciences Journal, 16(1), 41–51.

Samsonov, S. V., Feng, W., Blais-Stevens, A., & Eaton, D. W. (2024). Ground deformation due to natural resource extraction in the Western Canada Sedimentary Basin. Remote Sensing Applications: Society and Environment, 34, 101159. https://doi.org/10.1016/j.rsase.2024.101159

Suesse, T., Brenning, A., & Grupp, V. (2023). Spatial linear discriminant analysis approaches for remote-sensing classification. Spatial Statistics, 57, 100775. https://doi.org/10.1016/j.spasta.2023.100775

Triyatno., Berti, I., Idris., Hermon, D., & Putra, A. (2020). Hazards and morphometry to predict the population loss due of landslide disasters in Koto XI Tarusan - Pesisir Selatan. *International Journal of GEOMATE*, 19(76), 98–103. https://doi.org/10.21660/2020.76.ICGeo12

Verma, S., Khalkho, D., & Gupta, L. K. (2020). Morphometric Analysis of a Drainage Basin using Remote Sensing and Geographical Information System (GIS). International Journal of Current Microbiology and Applied Sciences, 9(4), 1950–1959. https://doi.org/10.20546/ijcmas.2020.904.232

Yang, T. Y., Lepine-Lacroix, S., Guerrero, J. A. R., McFadden, J. B. W., & Al-Janabi, M. A. Q. (2022). Seismic performance evaluation of innovative balloon type CLT rocking shear walls. Resilient Cities and Structures, 1(1), 44–52. https://doi.org/10.1016/j.rcns.2022.03.004

Zocchi, M., Masciulli, C., Mastrantoni, G., Troiani, F., Mazzanti, P., & Scarascia Mugnozza, G. (2025). Automatic landslide prioritization at regional scale through PS-InSAR cluster analysis and socio-economic impacts. Remote Sensing Applications: Society and Environment, 37, 101414. https://doi.org/10.1016/j.rsase.2024.101414